BIOCHEMISTRY

Article

Tryptophan Scanning Mutagenesis in the TM3 Domain of the *Torpedo californica* Acetylcholine Receptor Beta Subunit Reveals an □-Helical Structure

John Santiago, Gisila R. Guzmn, Karla Torruellas, Legier V. Rojas, and Jos A. Lasalde-Dominicci

Biochemistry, **2004**, 43 (31), 10064-10070 • DOI: 10.1021/bi0362368

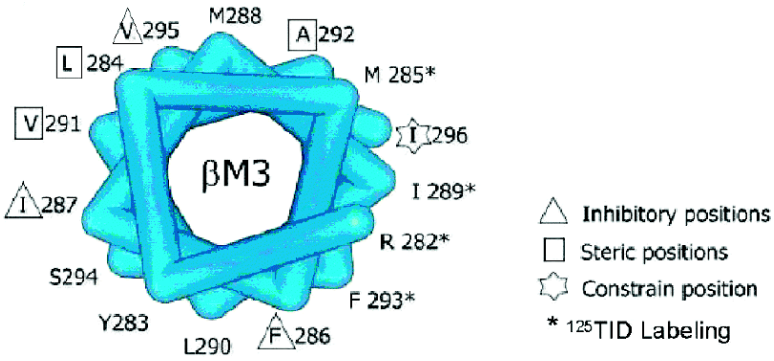

More About This Article

Additional resources and features associated with this article are available within the HTML version:

- Supporting Information
- Access to high resolution figures
- Links to articles and content related to this article
- Copyright permission to reproduce figures and/or text from this article

View the Full Text HTML

Tryptophan Scanning Mutagenesis in the TM3 Domain of the *Torpedo californica* Acetylcholine Receptor Beta Subunit Reveals an α-Helical Structure†

John Santiago,‡ Gisila R. Guzmán,‡ Karla Torruellas,‡ Legier V. Rojas,§ and José A. Lasalde-Dominicci*,‡

Department of Biology, University of Puerto Rico, P.O. Box 23360, San Juan, Puerto Rico 00931-3360, and Department of Physiology, School of Medicine, Universidad Central del Caribe, Bayamon, Puerto Rico 00960-6032

Received December 12, 2003; Revised Manuscript Received April 14, 2004

ABSTRACT: We used tryptophan substitutions to characterize the beta M3 transmembrane domain (βTM3) of the acetylcholine receptor (AChR). We generated 15 mutants with tryptophan substitutions within the βTM3 domain, between residues R282W and I296W. The various mutants were injected into *Xenopus* oocytes, and expression levels were measured by [^{125}I]-α-bungarotoxin binding. Expression levels of the M288W, I289W, L290W, and F293W mutants were similar to that of wild type, whereas the other mutants (R282W, Y283W, L284W, F286W, I287W, V291W, A292W, S294W, V295W, and I296W) were expressed at much lower levels than that of wild type. None of these tryptophan mutants produced peak currents larger than that of wild type. Five of the mutants, L284W, F286W, I287W, V295W, and I296W, were expressed at levels <15% of the wild type. I296W had the lowest expression levels and did not display any significant ACh-induced current, suggesting that this position is important for the function and assembly of the AChR. Tryptophan substitution at three positions, L284, V291, and A292, dramatically inhibited AChR assembly and function. A periodicity analysis of the alterations in AChR expression at positions 282−296 of the βTM3 domain was consistent with an α-helical structure. Residues known to be exposed to the membrane lipids, including R282, M285, I289, and F293, were all found in all the upper phases of the oscillatory pattern. Mutants that were expressed at lower levels are clustered on one side of a proposed α-helical structure. These results were incorporated into a structural model for the spatial orientation of the TM3 of the *Torpedo californica* β subunit.

The nicotinic acetylcholine receptor (AChR)[1] from muscle and *Torpedo* electroplax is an integral membrane protein comprised of four homologous polypeptide subunits in the stoichiometry of α2βγδ (*1*−*5*). A model for the AChR topology obtained from hydrophobicity profiles indicates that each of the subunits possesses at least four transmembrane domain regions, designated as M1, M2, M3, and M4 (or TM1 to TM4), with both N- and C-termini located on the extracellular side (*6*, *7*). Most of the studies that have characterized the role of these transmembrane domains have focused on the TM2 domain (*8*−*18*). Of these putative transmembrane regions, the TM2 and TM1 segments from each subunit participate in forming the wall-lining pore of the ion channel. The TM3 and TM4 regions have the most contact with the lipid interface (*19*, *20*). The TM4 domain is the most hydrophobic, and its side chains are the least conserved. It has been shown that mutations of lipid-exposed residues within TM4 can dramatically alter the AChR channel gating kinetics (*21*−*26*).

Analysis of TM3 demonstrated that this lipid-exposed domain is a key component of the AChR channel gating machinery. Wang and co-workers found that the V285I mutation in TM3 in the muscle-type α-subunit causes a congenital myasthenic syndrome (*27*). Tryptophan substitutions at the lipid-exposed positions within TM3 of the γ-subunit have been reported to increase the macroscopic response of the *Torpedo* AChR (*28*). Furthermore, replacement with hydrophobic amino acids at the 8′ position of TM3 of the muscle-type AChR further suggested that this domain contributes to the channel gating (*29*). A more recent study provided additional evidence suggesting that the αTM3 domain plays a role in channel gating and that lipid-exposed domains within this region regulate the differential modulation of ion channel function in various AChR species (*30*). These previous studies clearly indicate that the TM3 transmembrane domain plays an important role in the AChR gating mechanism. However, the detailed secondary structure and spatial orientation of this transmembrane segment remain unknown.

The three-dimensional organization of the AChR has been characterized at 9 Å resolution by electron microscopy of tubular crystals of *Torpedo* postsynaptic membranes embedded in amorphous ice (*2*). At this resolution, a single rod was visible around the central axis of the transmembrane

† This research was supported by National Institutes of Health Grants 2GM56371-05 GM08102-27 and by RCMI-G12RR03035-16. John Santiago was supported by the Puerto Rico NSF-EPSCoR Grant EPS-97478, and Gisila Guzmán by the MBRS−RISE Program 5R25GM61151.

* Corresponding author. Telephone: (787) 764-0000-2765/4887. Fax: (787) 753-3852. E-mail: joseal@coqui.net.

‡ University of Puerto Rico.

§ Universidad Central del Caribe.

[1] Abbreviations: AChR, nicotinic acetylcholine receptor; ACh, acetylcholine; TM, transmembrane domain.

10.1021/bi0362368 CCC: $27.50
Published on Web 07/15/2004

domain (presumably TM2) within each subunit, suggesting that TM2 is the only transmembrane segment that forms an α-helical structure. Due to the absence of similar density within the lipid-facing portion of the AChR, it was originally suggested that the TM1, TM3, and TM4 domains existed in a β-sheet structure (*2*). In a more recent study, the same authors provided a new interpretation where all transmembrane segments were proposed to be α-helical structures (*31*). The pattern of labeling of TM3 and TM4 with the photoactivated hydrophobic probe 3-(trifluoromethyl)-3-m-[^{125}I]-iodophenyldiazirine ([^{125}I]-TID) was found to be consistent with an α-helical structure (*19*, *20*). Fourier transform infrared (FTIR) spectroscopy studies of receptors in which the extracellular and intracellular portions were removed by proteinase K digestion suggested that the transmembrane domains of the receptors include a mixture of α-helical and β structures (*32*). A more recent FTIR spectroscopy analysis of affinity-purified receptors, in which the nonmembrane domains were digested with Pronase and proteinase K, indicated that the secondary structures of the AChR transmembrane domains are predominantly α-helical (*33*). H NMR analysis of a three-dimensional structure of a synthetic polypeptide, corresponding to the αTM3 of *Torpedo*, suggested that this domain forms an α-helical structure (*34*). Moreover, tryptophan-scanning mutagenesis of the TM3 (*35*) and TM4 (*26*) transmembrane segments of the α subunit of the *Torpedo californica* AChR also suggests that both domains are α-helical structures.

In this study, we have characterized the TM3 transmembrane region of the β-subunit of the *T. californica* AChR. Fifteen positions (βR282 to βI296) of the putative βTM3 domain were sequentially replaced with tryptophan. The periodicity of receptor expression levels as a function of tryptophan substitution suggested that this region exists as an α-helical structure. Tryptophan replacements at three positions thought to be in contact with the lipid environment (M285, I289, and F293) resulted in AChR expression levels similar to that of the wild-type receptor. Tryptophan substitution at four positions presumed to be oriented toward the interior of the protein significantly inhibited channel function (L284, V291, and A292) and/or receptor assembly (I296). These results provide new information regarding the spatial orientation of the TM3 of the *T. californica* β subunit and its contribution to AChR assembly and function.

MATERIALS AND METHODS

Mutation of the β Subunit of the T. californica AChR. Site-directed mutagenesis of the β subunit of the AChR was carried out by mismatch amplification using two sequential rounds of polymerase chain reaction (PCR) (*36*). The coding region of the β subunit of *T. californica* AChR was subcloned from Pα (*37*) into the HindIII and EcoRI sites of the pGEM3Z(−) vector (Promega, Madison, WI). Mutagenic primers included the Trp codon (TGG) in place of the wild-type codon at the desired positions and extended 11−13 bases on each side of the mismatched region. The primers were synthesized by Gibco BRL (Gaithersburg, MD). Each PCR included 10 mM Tris-HCl (pH 8.3), 50 mM KCl, 1.5 mM $MgCl_2$, 0.01% gelatin, 200 nM of each deoxynucleotide, 100 ng of DNA template, 1 μM of each primer, and 2.0 units of Taq DNA polymerase (Promega, Madison, WI) in a final volume of 100 μL. Amplification reactions were performed in a DNA thermal cycler (Perkin-Elmer-Cetus) programmed for 30 cycles of a three-step protocol: 3 min at 94 °C, 1 min at 50 °C, and 3 min at 72 °C. The PCR reactions were subjected to electrophoresis on agarose gels, and the desired PCR products were excised from the gels and purified with Gene-Clean (Bio 101, La Jolla, CA). These mutant DNA fragments were then used in a second fusion PCR. The fusion product was purified from the gel with Gene-Clean and digested with BspE1 and Nco1 (New England BioLabs, Beverly, MA). The plasmid containing the coding region of the β subunit was also digested with BspE1 and Nco1. The mutant fragment was then inserted into the β subunit with T4 DNA ligase (New England Biolabs, Beverly, MA).

Tryptophan substitutions at positions R282, Y283, L284, F286, I287, L290, S294, and V295 were created using the QuickChange site-directed mutagenesis kit (Stratagene, La Jolla, CA). Mutations were confirmed by sequence analysis performed at the DNA Sequencing Facility in the Section of Evolution and Ecology, University of California, Davis, CA. To exclude the possibility of secondary mutations, the entire coding region of the β subunit was subjected to DNA sequence analysis. For mutations prepared by mismatch amplification or overlap extension, the entire mutagenized fragment was sequenced from both the 3′ and 5′ directions.

Expression in Xenopus laevis Oocytes. RNA transcripts were synthesized in vitro as described previously *(21)*. Briefly, RNA transcripts corresponding to the α, β, γ, and δ subunits were injected in *Xenopus* oocytes in a 2:1:1:1 ratio (10 ng/oocyte at a concentration of 0.2 μg/μL).

Voltage Clamping. Three days after mRNA injection, ACh-induced currents were recorded with a two-electrode voltage clamp using the Gene Clamp 500 amplifier (Axon Instruments, Foster City, CA). Electrodes were filled with 3 M KCl, and resistances were <2 MΩ. Impaled oocytes in the recording chamber were perfused at a rate of 0.5 mL/s with MOR-2 buffer [115 mM NaCl, 2.5 mM KCl, 5 mM $MgCl_2$, 1 mM Na_2HPO_4, 5 mM *N*-(2-hydroxyethyl)piperazine-*N*′-2-ethanesulfonic acid (HEPES), and 0.2 mM $CaCl_2$ (pH 7.4)]. To determine dose−response curves for each oocyte, membrane potential was held at −70 mV. Membrane currents were sampled at 4 kHz and filtered at 2 kHz using the DigiData 1200 interface (Axon Instruments, Union City, CA). The Whole Cell Program 2.3 (kindly provided by Dr. J. Dempster, University of Strathclyde, U.K.) running on a Pentium III-based computer was used for data acquisition. Prism version 3.0 (GraphPAD Software, San Diego, CA) software was utilized for data analysis and curve fitting. Peak currents at six ACh concentrations (1−300 μM) were used to produce the dose−response curves. The data for the dose−response curves were fit using a curve of the form $Y = 100/[1 + (EC_{50}/A)^n]$. The EC_{50} and Hill coefficient values for individual oocytes were averaged to generate final estimates.

[^{125}I]-α-Bungarotoxin Binding Assay. The expression of nAChR in the oocyte membrane was determined by measuring the binding of [^{125}I]-α-bungarotoxin (Amersham Life Sciences, Arlington Heights, IL) to intact oocytes, as described previously *(21)*. After macroscopic currents were recorded, four to twelve oocytes expressing each mutation were incubated in 10 nM [^{125}I]-α-bungarotoxin ([^{125}I]-BTX) with 5 mg/mL bovine serum albumin in MOR-2 at room temperature for 2 h. Excess toxin was then removed by washing five times with 1 mL of MOR-2. To determine the

Table 1: Functional Analysis of βM3 Mutants[a]

nAChR type	expression level (fmol)	EC_{50} (μM)	Hill coeficient	I_{max} (nA)	normalized response (nA/fmol)
wild type	4.1 ± 0.7	20 ± 2	1.4 ± 0.3	2285 ± 354	606 ± 58
R282W	0.9 ± 0.2[c]	30 ± 1[c]	1.17 ± 0.03	1934 ± 336	2506 ± 473[d]
Y283W	1.3 ± 0.2[c]	13 ± 3	1.24 ± 0.07	1038 ± 264[b]	754 ± 107
L284W	0.30 ± 0.05[d]	45 ± 4[d]	1.37 ± 0.09	209 ± 70[d]	810 ± 157
M285W	6 ± 1[c]	42 ± 6[d]	1.4 ± 0.1	1031 ± 173[c]	217 ± 56[d]
F286W	0.3 ± 0.1[c]	49 ± 2[d]	1.31 ± 0.02	465 ± 56[c]	2091 ± 662[c]
I287W	0.64 ± 0.06[d]	45 ± 3[d]	1.34 ± 0.08	785 ± 105[c]	1224 ± 129[d]
M288W	2.6 ± 0.6	17 ± 3	1.28 ± 0.04	672 ± 137[b]	259 ± 18[c]
I289W	3 ± 2	76 ± 6[d]	1.24 ± 0.08	859 ± 262[c]	339 ± 79[b]
L290W	3 ± 0.8	18 ± 2	1.13 ±0.08	1797 ± 345	915 ± 202
V291W	1.1 ± 0.4[c]	ND	ND	182 ± 51[d]	158 ± 41[d]
A292W	1.3 ± 0.1[b]	ND	ND	83 ± 17[c]	67 ± 18[d]
F293W	2.3 ± 0.3	16 ± 3	1.2 ± 0.1	1158 ± 139[b]	477 ± 28
S294W	1.6 ± 0.2[b]	6.5± 0.5[d]	1.1 ± 0.1	2065 ± 229[c]	1301 ± 82[d]
V295W	0.4 ± 0.1[c]	8.3± 0.6[d]	1.8 ± 0.4	1217 ± 241[b]	4201± 1240[d]
I296W	0.26 ± 0.06[d]	ND	ND	ND	(3 of 7) 107 ± 26
I289W/F293W	NE	ND	ND	ND	ND

[a] Four to twelve oocytes were used for each set of voltage clamp experiments and α-BuTX binding. Values are expressed as the mean ± the standard error. The normalized response for each oocyte was obtained from the ACh-induced current at 300 μM divided by the femtomoles within the same oocyte. ND = no detectable current; NE = no expression. [b] $p < 0.01$. [c] $p < 0.05$. [d] $p < 0.001$.

normalized functional response to ACh, [^{125}I]-BTX binding was analyzed immediately after voltage clamping using a Beckman Gamma 5500. Noninjected oocytes were used as a control to determine background nonspecific binding. The standard curve was defined by counting 0−20 μL of 1 nM [^{125}I]-BTX solution (equivalent to 0−20 fmol). Using this approach, the normalized channel response to ACh-induced current (nanoamperes) per femtomole of surface α-BTX binding sites was determined.

Modeling Methods. The structural models for the βTM3 domain was examined using Biomer V1.0 alpha (see http://www.scripps.edu/n~nwhite/B). The structures were minimized using the Fletcher−Reeves conjugated gradient algorithm (<2000 iterations). The minimized pdb structures generated in Biomer V1.0 alpha were then analyzed using Accelrys DS ViewerPro 5.0 (www.accelrys.com). The periodicity values for the expression levels of βTM3 mutants were estimated by performing the first derivative for each amino acid position and estimating the distance between the zeros for all positions using Graph Pad Software.

RESULTS

Expression of βM3 Mutants. Fifteen residues, from R282 to I296, within the TM3 domain of the β subunit of *T. californica* AChR were individually replaced with tryptophan. One double tryptophan mutant, I289W/L293W, was also generated. mRNA transcripts were synthesized and injected into *X. laevis* oocytes, and the level of cell-surface expression of mutant AChRs was assessed by ^{125}I-BTX binding analysis, as described in Materials and Methods. The M288W, I289W, L290W, and F293W mutants were expressed at levels similar to that of wild type (Table 1). The L284W, F286W, I287W, V295W, and I296W mutants were expressed at the lowest levels (<15% of wild-type expression levels). The M285W mutant was expressed at somewhat higher levels than wild type, and the double mutant I289W/L293W exhibited no detectable ^{125}I-BTX binding on the surface of oocytes. These results suggest that the βTM3 transmembrane domain can tolerate a single substitution of a bulky hydrophobic side chain at all 15 positions but cannot tolerate a double tryptophan substitution at positions I289 and F293 (see Table 1).

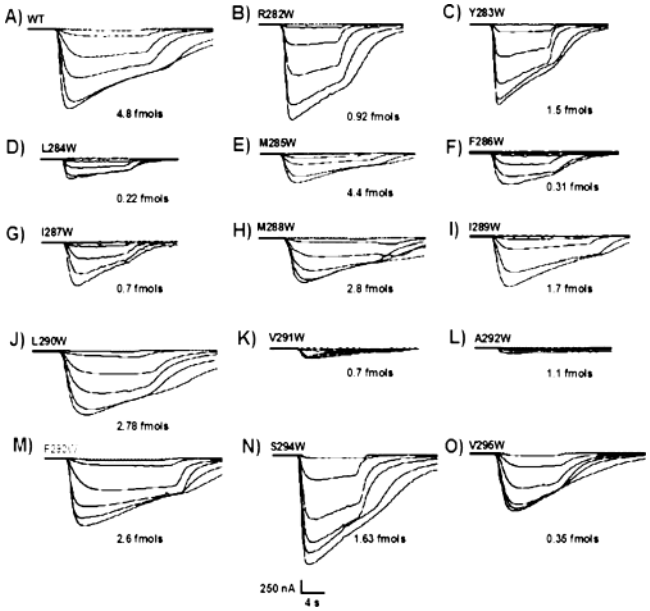

FIGURE 1: Macroscopic-current responses of wild type and βM3 mutants. Families of macroscopic currents derived from individual *Xenopus* oocytes for (A) wild type and each of the following βM3 mutants: (B) R282W; (C) Y283W; (D) L284W; (E) M285W; (F) F286W; (G) I287W; (H) M288W; (I) I289W; (J) L290W; (K) V291W; (L) A292W; (M) F293W; (N) S294W; (O) V295W. Currents were recorded using a two-electrode voltage clamp, as described in MATERIALS AND METHODS. ACh-induced currents were detected at a membrane potential of −70 mV, digitized at 4 kHz and filtered at 2 kHz. The ACh concentrations used to generate the families of currents were 1, 3, 10, 30, 100, and 300 μM. After the macroscopic currents were recorded, the level of AChRs expressed at the oocyte surface was normalized to the surface α-BTX binding for each individual oocyte. The corresponding expression levels of AChRs for each individual oocyte tested are shown for each family of currents (in femtomoles).

Electrophysiological Characterization of the βM3 Mutants: Effect on Macroscopic Current Response. Figure 1 shows families of current traces elicited by progressive increases in ACh concentration (1, 3, 10, 30, 100, and 300

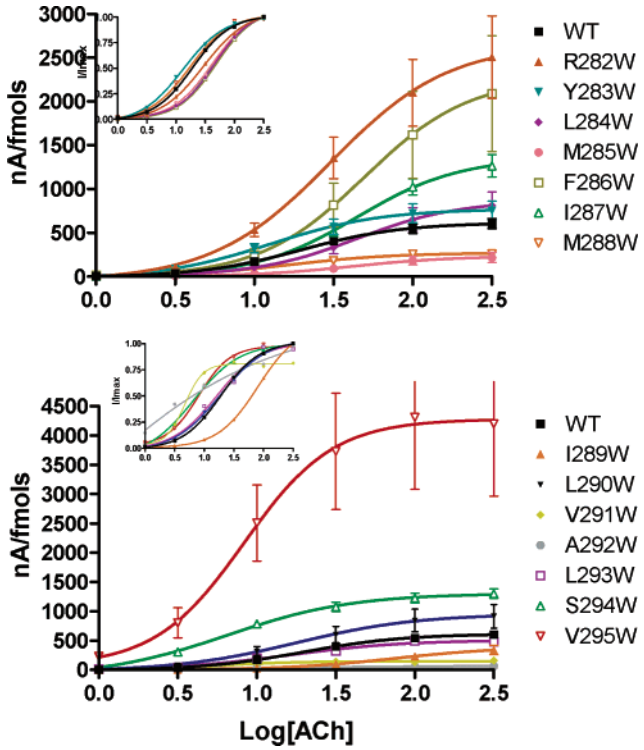

FIGURE 2: Dose−response curves of wild type and βM3 mutant AChRs. Data are expressed as ACh-induced currents (nA) per femtomole of surface α-BTX binding sites. The inset shows dose−response curves normalized to maximum current. (A, top) Dose−response curves for oocytes expressing wild type and mutants R282W to M288W. (B, bottom) Dose−response curves for oocytes expressing wild type and mutants I289W to V295W. The current values used were collected from peak currents at six ACh concentrations (1−300 μM) and fitted using a curve of the form $Y = 100/[1 + (EC_{50}/A)^n]$. For each ACh concentration, the standard error of the mean (±SEM) was determined from four to twelve individual oocytes in each group.

μM at −70 mV) for the wild-type AChR and each of the βTM3 mutants. None of the mutants produced peak currents larger than that of wild type. However, five of the mutants exhibited significantly higher normalized macroscopic currents, as compared to wild type (606 nA/fmol): R282W (2506 nA/fmol), F286W (2091 nA/fmol), I287W (1224 nA/fmol), S294W (1301 nA/fmol), and V295W (4201nA/fmol). On the other hand, three of the mutants showed significantly reduced normalized responses: M285W (217 nA/fmol), M288W (259 nA/fmol), and I289W (339 nA/fmol). The remaining three mutants, V291W, A292W, and I296W, exhibited extremely small currents.

Effects of Mutations on the EC_{50} and Hill Coefficient Values for ACh. ACh dose−response curves for the βM3 mutations are shown in Figure 2. The EC_{50} values for wild type and the various βM3 mutants are shown in Table 1. The R282W, L284W, M285W, F286W, I287W, and I289W mutants exhibited 2- to 3-fold higher EC_{50} values for ACh, as compared to wild type. The EC_{50} values of Y283W, M288W, L290W, and L293W were similar to that of wild type. Only two of the mutants, S294W and V295W, had EC_{50} values that were significantly lower than that of wild type. The decreased EC_{50} for ACh exhibited by the S294W and V295W mutants is consistent with the increased normalized response of these mutants. The EC_{50} and Hill coefficient values could not be estimated for the V291W, A292W, and I296W mutants, due to the extremely low currents exhibited by these receptors. No significant changes in the Hill coefficients were observed in any of the other twelve mutants, as compared to wild type. These results indicate that these mutations do not alter the cooperativity of ACh binding to the AChR.

DISCUSSION

Previous studies demonstrated that tryptophan substitution at lipid-exposed positions dramatically affects the macroscopic response and channel gating kinetics of the AChR (*21*−*26*, *28*). In the current study, [^{125}I-α-BTX] binding analysis of wild type and mutant AChR expression in *X. laevis* oocytes demonstrated that tryptophan residues can be accommodated along the βTM3 domain except at position I296.

Functional Interpretation. Our previous studies showed that tryptophan substitutions at lipid-exposed positions within the αM4 (*21*−*22*, *26*), γM3 (*28*), and αTM3 (*30*, *35*) domains can significantly increase the normalized macroscopic response of the AChR. None of the tryptophan mutants generated in the present study produced peak currents larger than that of wild type. Tryptophan substitutions at five positions of the βM3 transmembrane segment (R282W, F286W, I287W, S294W, and V295) induced an apparent increase in the normalized response of the AChR (Table 1). Mutations R282W, F286W, and I287W exhibited EC_{50} values higher than that of wild type, suggesting a diminished functional response. As shown in Table 1, R282W, F286W, and I287W were expressed at much lower levels (0.9, 0.3, and 0.64 fmol, respectively) than wild type. In contrast, S294W and V295W exhibited EC_{50} values that were significantly lower than that of the wild type receptor, suggesting that these AChR mutations induce a gain-in-function response. This result appears to be consistent with the observed increase in macroscopic response; however, single channel data analysis will be necessary to verify this hypothesis. Tryptophan replacement at position M285, which presumably faces the lipid environment (*20*), resulted in a 3-fold reduction in the normalized response. Interestingly, only the M285W mutant exhibited a significant increase in AChR expression levels, as compared to wild type.

In contrast to the aforementioned mutations, the V291W and A292W mutations exhibited the largest reduction in macroscopic current response among the various mutants in this study (Figure 1). The average expression level for these two mutants was >1.0 fmol, which is considerably higher than that of mutants that exhibited the largest normalized macroscopic responses (i.e., V295W, 0.43 fmol, and F286W, 0.34 fmol). Therefore, the tryptophan-induced increase in side chain volume at positions V291 and A292 is likely to impair normal channel gating. Although the V295W had the highest normalized response among all the βTM3 mutants, the peak current (1217 nA) and expression level (0.4 fmol) of this mutant were significantly lower than those of wild type; therefore, this was considered to be an inhibitory position. Independent photolabeling studies did not detect labeling at this position (*20*), suggesting that it might face neighboring transmembrane segments toward the interior of the protein. According to the most recent AChR structure (*31*), V295 partially faces toward the αTM1 domain and is less oriented toward the βTM2 domain than V291.

Interpretation of Normalized Macroscopic Response. The higher normalized macroscopic responses observed in the mutants discussed above are not necessarily due to their low expression levels, because other mutants with similar expression levels (i.e., L284W) did not exhibit normalized responses that were higher than those of wild type. The data that we have gathered thus far indicate that mutations within TM3 and TM4 do not affect agonist binding nor do they produce global changes in the AChR ion channel pore, as they have no effects on single channel conductance, reversal potentials, or calcium permeability *(21*−*23, 30, 38)*. A previous study by Dr. Gary Yellen's group demonstrated that the affinity of α-BTX binding to the AChR is not affected by mutations within the agonist binding site *(39)*. Thus, it is very unlikely that α-BTX binding affinity is altered in response to these mutations made within *β*TM3. Accordingly, the pattern of the normalized response seems to depend on the mutant itself, rather than on variation in expression levels. It is important to understand that the normalized response is a measure of the ratio of the fraction of functional surface AChRs to the total number of ^{125}I-α-BTX-labeled receptors (both silent and functional). It has been demonstrated that the fraction of functional surface AChRs (N_f) to the total number of surface α-BTX-AChRs (both silent and functional, or N_t) is much less than 1.0 in the chick ciliary ganglion *(40)*. Previously, we have hypothesized that a particular mutation could alter the equilibrium between the silent and functional pools of receptors (*26*), which could explain the pattern of normalized responses observed for the R282W, F286W, and I287W mutants. To test this hypothesis, it is necessary to fully understand the factors that control how receptors move between the silent and functional surface pools of AChRs. In the present study, we used the normalized macroscopic response as a quantitative measure of the macroscopic response of AChR mutants. To demonstrate that a particular mutant exhibits an increased or decreased normalized macroscopic response, it will be necessary to correlate single channel analysis with the macroscopic data.

Structural Interpretation. Figure 3A shows the periodicity profile of changes in AChR expression levels as a function of tryptophan replacement at various positions in the *β*TM3 transmembrane segment. The curve shows that the oscillations of periodicity are approximately 3.6 amino acids. As shown in Figure 3A, the largest shift in expression levels occurs in the second phase of the oscillatory diagram, corresponding to positions 284, 285, and 286. This expression pattern suggests that these residues (L284, M285, and F286) are likely to exist in a tightly packed α-helical structure. It is possible that residues 284−286 form a 3_{10} α-helical structure. After the first stretch of residues (284−286), there are two other well-defined oscillations, 287−291 and 292−295. These two oscillatory patterns are slightly less defined than 284−286 but are still consistent with an α-helical structure. Although the oscillatory profile strongly suggests that the *β*TM3 domain forms an α-helical structure, there could be a small distortion in the center of the helix (phase III in Figure 3A). It is possible that the flattened area in the center of the helix is caused by a twist resulting from the crossing angle of the *β*TM3 helix with other neighboring helices (*41*). Remarkably, residues that are exposed to the membrane lipids (*19*−*20*) were found in all the upper phases of the oscillatory pattern, including I (R282), II (M285), III (I289), and IV (F293). Our current findings provide additional experimental evidence for a potential α-helical structure within the *Torpedo* *β*TM3 domain. Mutants that are expressed at lower levels are clustered on one side of a postulated α-helical structure. As shown in the helical diagram in Figure 3B, L284W, F286W, and I287W, which were expressed at levels <15% of the wild type, are clustered facing the opposite side of the F293, R282, I289, and M285 residues, which have been shown to be exposed to the lipid. We considered the possibility that *β*TM3 could have a *β*-sheet structure; however, the data were not consistent with a *β*-sheet structure for the following reasons. First, a tryptophan substitution would be expected to increase expression levels at alternate positions along the peptide chain, and this was not observed. Second, in a *β*-structure, a residue like V291W must be oriented toward the lipid environment, as are M285, I289, and F293. The V291W residue is actually located in the lower side of phase III (Figure 3A). Taken together, our data and previous photo-

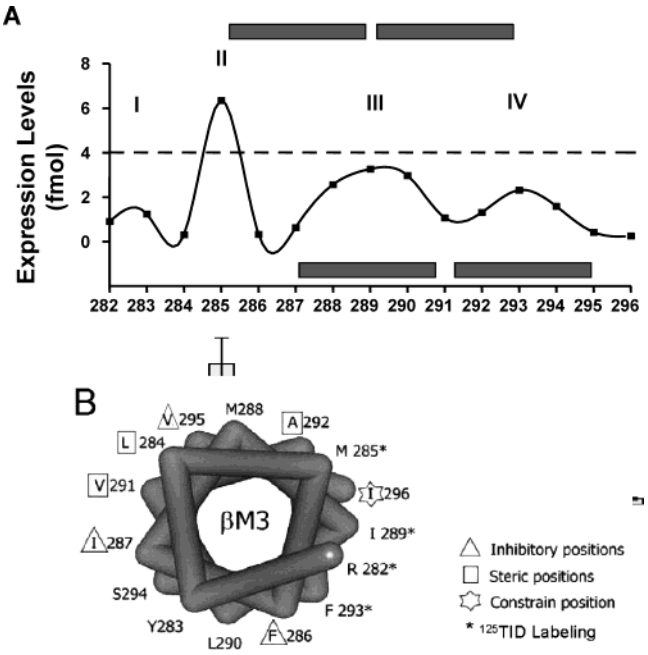

FIGURE 3: (A) Periodicity of changes in expression of AChR as a function of tryptophan substitution in the *β*M3 transmembrane segment. Individual sets of data for the expression of each *β*M3 AChR mutant are shown as boxes, expressed as average femtomoles ± SEM. The curves display an oscillation with a periodicity of approximately 3.6 amino acids. The gray bar represents 3.6 amino acids, and the dashed line represents the wild-type expression levels. Roman numerals above the curve indicate the phases of the periodicity profile. The plot of expression levels versus the mutant position within *β*M3 was constructed using a cubic spline curve regression function (Prism version 3.0, GraphPAD Software). The periodicity value was estimated by performing the first derivative for each amino acid position and estimating the distance between the zeros for all positions using Graph Pad Software. Each point on the *Y*-axis represents an average of a number of measurements (see Table 1). (B) Helical wheel diagram (view from top) for an α-helical representation (3.6 amino acids per turn) of the *β*M3 showing the location of steric, constraint, inhibitory, and lipid-exposed positions (*20*) according to the present mutagenesis study. Positions at which tryptophan substitution results in relatively normal AChR expression levels compared to wild type, including M285, I289, and F293, are oriented toward the same face of the α-helix. The asterisk (*) indicates that the residue was presumably exposed to the lipid environment, as demonstrated by independent photolabeling studies (*20*).

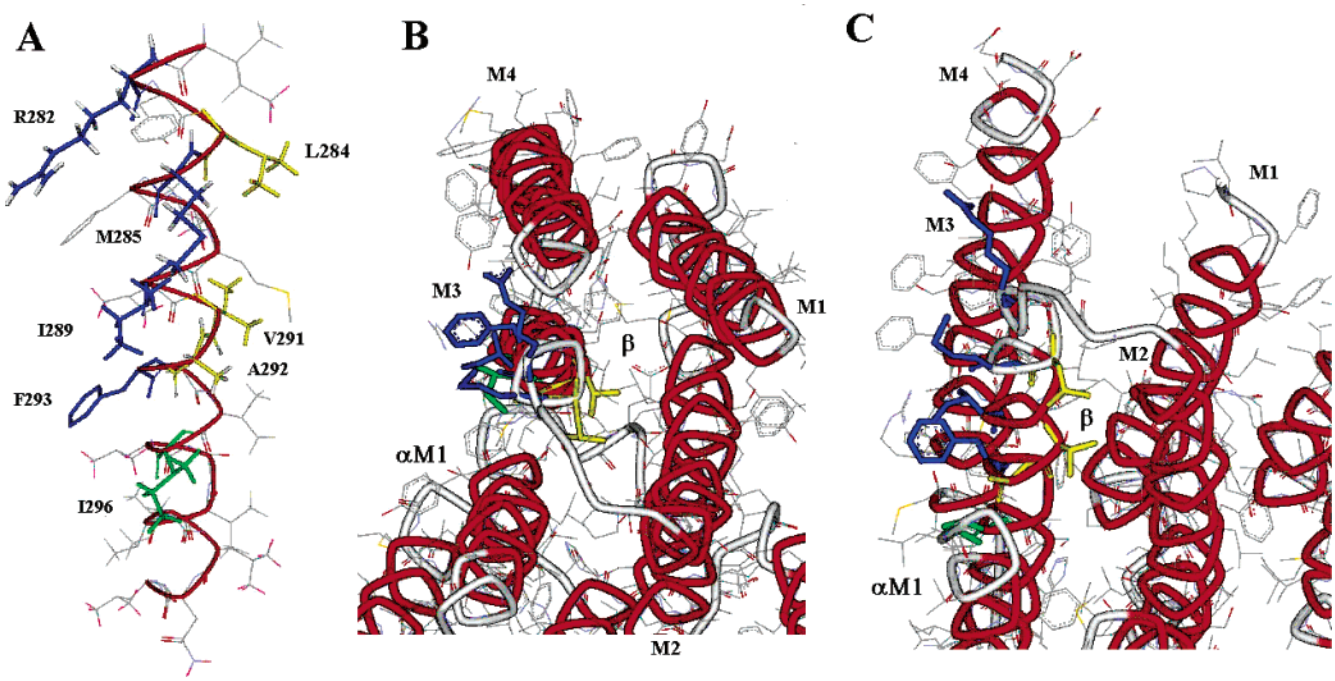

FIGURE 4: Structural model of the βM3 domain of the *Torpedo californica* AChR according to the present study (A) and according to a recent structure by Miyazawa et al. (2003) (B and C). (A) Molecular modeling from the extended conformation of the βM3 domain starting at positions 282 through L304 using a clockwise rotation and 3.6 amino acids per helical turn. (B) Helical view from the top. (C) Side view of the βM3 according to ref 31. Labeled residues in blue (R282, M285, I289, and F293) have been shown to be in contact with the lipid interface (*20*). Steric positions V291 and A292 are shown in yellow, and constraint position I296 is shown in green (in parts B and C hydrogens on side chains are not shown).

labeling studies by Cohen's group (*20*) are not consistent with a β-sheet structure.

Constraint and Steric Sites. The I296W mutant exhibited remarkably low expression levels (see Table 1), suggesting that there is a structural constraint at this position that is critical for receptor assembly and/or oligomerization. The lack of ion channel function in this mutant is likely to result from problems with receptor assembly. The present data suggest that there is a structural constraint in I296W that is critical for assembly and oligomerization of the receptor; therefore, we designated this position as a constraint site. Previously, we found a similar structural constraint at position I417 in the TM4 transmembrane segment of the α subunit of *T. californica* (*26*). The most recent structural model for the transmembrane segments of the AChR (*31*) suggests that position I296 is oriented toward the αTM1 transmembrane segment of one of the α-subunits in the closed state of the channel (see Figure 4B and C). It is possible that the increase in volume produced by a tryptophan substitution at position I296 could produce a structural constraint with residues of the αTM1 domain. For example, according to the recently proposed AChR structure (*31*), residue L224 in the αTM1 domain could exist in very close proximity to a tryptophan at I296.

At positions L284, F286, I287, and V295 (see Table 1), a tryptophan substitution decreased AChR expression levels to <15% of that of wild type, suggesting that receptor assembly and perhaps oligomerization are significantly affected by increases in side chain volume at these positions. In contrast, tryptophan substitutions at positions V291 and A292 resulted in significant reduction of AChR expression, but these mutations appeared to dramatically inhibit ion channel function. Therefore, we designated V291 and A292 as steric positions. Unlike the I296 position, V291 and A292 are oriented toward the interior of the protein (see Figure 4B), facing an open crevice in proximity to the M2 domain (*31*). The orientation of these two residues toward the ion channel domain is consistent with the remarkable inhibition of AChR channel function observed for the V291W and A292W mutants. Figure 4 shows the orientation of V291 and A292 (shown in yellow) according to the recent AChR structure (*31*) from top and side orientations. The periodicity analysis of the βM3 (Figure 3) predicts an α-helical structure, as shown in Figure 4A. The biochemical and electrophysiological characterization of these βTM3 mutants is consistent with an α-helical structure, and this is also consistent with the recently proposed nAChR structure (*31*). Furthermore, the electrophysiological characterization of the present mutations defined positions within the βTM3 domain that are critical for AChR assembly and function.

ACKNOWLEDGMENT

We especially thank José Reyes for his help in the construction of these mutants and Dr. Alejandro Ortiz-Acevedo for assistance with the molecular modeling and structural interpretation.

REFERENCES

1. Pradier, L., and McNamee, M. G. (1992) The nicotinic acetylcholine receptor, in *The Structure of Biological Membranes* (Yeagle, P., Ed.) 1st ed., pp 1047−1106, Telford Press, New Jersey.
2. Unwin, N. (1993) Nicotinic acetylcholine receptor at 9 Å resolution, *J. Mol. Biol. 229*, 1101−1124.
3. Karlin, A., and Akabas, M. H. (1995) Toward a structural basis for the function of nicotinic acetylcholine receptors and their cousins, *Neuron 15*, 1231−44.

4. Arias, H. R. (1998) Binding sites for exogenous and endogenous non-competitive inhibitors of the nicotinic acetylcholine receptor, *Biochim. Biophys. Acta 1376*, 173−220.
5. Changeux, J. P., and Edelstein S. J. (1998) Allosteric receptors after 30 years, *Neuron 21*, 959−980.
6. Noda, M., Takahashi, H., Tanabe, T., Toyosata, M., Kikyotani, S., Furutani, Y., Hirose, T., Takashima, H., Inayama, S., Miyata, T., and Numa, S. (1983) Structural homology of *Torpedo californica* acetylcholine receptor subunits, *Nature (London) 302*, 528−532.
7. Dipaola, M., Czajkowski, C., and Karlin, A. (1989) The sidedness of the COOH terminus of the acetylcholine receptor delta subunit, *J. Biol. Chem. 264*, 15457−15463.
8. Giraudat, J., Dennis, M., Heidmann, T., Chang, J. Y., and Changeux, J. P. (1986) Structure of the high-affinity binding site for noncompetitive blockers of the acetylcholine receptor: serine-262 of the delta subunit is labeled by [^{3}H]chlorpromazine, *Proc. Natl. Acad. Sci. U.S.A. 83*, 2719−2723.
9. Giraudat, J., Dennis, M., Heidmann, T., Hamont, P. Y., Lederer, F., and Changeux, J. P. (1987) Structure of the high-affinity binding site for noncompetitive blockers of the acetylcholine receptor: [^{3}H]chlorpromazine labels homologous residues in the beta and delta chains, *Biochemistry 26*, 2410−2418.
10. Giraudat, J., Gali, J., Revah, F., Changeux, J. P., Haumont, P., and Lederer, F. (1989) The noncompetitive blocker [^{3}H]chlorpromazine labels segment M2 but not segment M1 of the nicotinic acetylcholine receptor alpha-subunit, *FEBS Lett. 253*, 190−198.
11. Hucho, F., Oberthur, W., and Lottspeich, F. (1986) The ion channel of the nicotinic acetylcholine receptor is formed by the homologous helices M II of the receptor subunits, *FEBS Lett. 205*, 137−142.
12. Imoto, K., Methfessel, C., Sakmann, B., Mishina, M., Mori, Y., Konno, T., Fukuda, M., Kurasaki, M., Bujo, H., Fujita, Y., and Numa, S. (1986) Location of a delta-subunit region determining ion transport through the acetylcholine receptor channel, *Nature 324*, 670−674.
13. Imoto, K., Busch, C., Sakmann, B., Mishina, M., Konno, T., Nakai, J. M., Bujo, H., Mori, Y., Fukuda, M., and Numa, S. (1988). Rings of negatively charged amino acids determine the acetylcholine receptor channel conductance, *Nature 335*, 645−648.
14. Imoto, K., Konno, T., Nakai, J., Wang, F., Mishina, M., and Numa, S. (1991) A ring of uncharged polar amino acids as a component of channel constriction in the nicotinic acetylcholine receptor, *FEBS Lett. 289*, 193−200.
15. Charnet, P., Labarca, C., Leonard, R. J., Vogelaar, N. J., Czyzyk, L., Gouin, A., Davison, N., and Lester, H. A. (1990) An open-channel blocker interacts with adjacent turns of alpha-helices in the nicotinic acetylcholine receptor, *Neuron 4*, 87−95.
16. White, B. H., and Cohen, J. B. (1992) Agonist-induced changes in the structure of the acetylcholine receptor M2 regions revealed by photoincorporation of an uncharged nicotinic noncompetitive antagonist, *J. Biol. Chem. 267*, 15770−15783.
17. Villarroel, A., and Sakmann, B. (1992) Threonine in the selectivity filter of the acetylcholine receptor channel, *Biophys. J. 62*, 196; 205−208.
18. Akabas, M. H., and Karlin, A. (1995) Identification of acetylcholine receptor channel-lining residues in the M1 segment of the alpha-subunit, *Biochemistry 34*, 12496−12500.
19. Blanton, M. P., and Cohen, J. B. (1992) Mapping the lipid-exposed regions in the *Torpedo californica* nicotinic acetylcholine receptor, *Biochemistry 31*, 3738−3750.
20. Blanton, M. P., and Cohen J. B. (1994) Identifying the lipid−protein interface of the *Torpedo* nicotinic acetylcholine receptor: secondary structure implications, *Biochemistry 33*, 2859−2872.
21. Lee, Y.-H., Li, L., Lasalde, J. A., Rojas, L. V., McNamee, M., Ortiz-Miranda, S. I., and Pappone, P. (1994) Mutations in the M4 domain of *Torpedo californica* acetylcholine receptor dramatically alter ion channel function, *Biophys. J. 66*, 646−653.
22. Lasalde, J. A., Tamamizu, S., Butler, D. H., Vibat, C. R. T., Hung, B., and McNamee, M. G. (1996) Tryptophan substitutions at the lipid-exposed transmembrane segment M4 of *Torpedo californica* acetylcholine receptor govern channel gating, *Biochemistry 35*, 14139−14148.
23. Ortiz-Miranda, S. I., Lasalde, J. A., Pappone, P. A., and McNamee, M. G. (1997) Mutations in the M4 domain of the *Torpedo californica* nicotinic acetylcholine receptor alter channel opening and closing, *J. Membr. Biol. 158*, 17−30.
24. Bouzat, C., Roccamo, A. M., Garbus, I., and Barrantes, F. J. (1998) Mutations at lipid-exposed residues of the acetylcholine receptor affect its gating kinetics, *Mol. Pharmacol. 54*, 146−153.
25. Tamamizu, S., Lee, Y.-H., Hung, B., McNamee, M. G., and Lasalde-Dominicci, J. A. (1999) Alteration in ion channel function of mouse nicotinic acetylcholine receptor by mutations in the M4 transmembrane domain, *J. Membr. Biol. 170*, 157−164.
26. Tamamizu, S., Guzmán, G., Santiago, J., Rojas, L. V., McNamee, M. G., and Lasalde-Domicci, J. A. (2000) Functional effects of periodic tryptophan substitutions in the alpha M4 transmembrane domain of the *Torpedo californica* nicotinic acetylcholine receptor, *Biochemistry 39*, 4666−4673.
27. Wang, H. L., Milone, M., Ohno, K., Shen, X., Tsujino, A., Batocchi, A. P., Tonali, P., Brengman, J., Engel, A. G., and Sine, S. M. (1999) Acetylcholine receptor M3 domain: stereochemical and volume contributions to channel gating, *Nature Neurosci. 2*, 226−233.
28. Cruz-Martin, A., Mercado, J. L., Rojas, L. V., McNamee, M. G., and Lasalde-Dominicci, J. A. (2001) Tryptophan substitutions at lipid-exposed positions of the gamma M3 transmembrane domain increase the macroscopic ionic current response of the *Torpedo californica* nicotinic acetylcholine receptor, *J. Membr. Biol. 183*, 61−70.
29. De Rosa, M. J., Rayes, D., Spitzmaul, G., and Bouzat, C. (2002) Nicotinic receptor M3 transmembrane domain: position 8′ contributes to channel gating, *Mol. Pharmacol. 62*, 406−414.
30. Navedo, M., Nieves, M., Rojas, L., and Lasalde-Dominicci, J. (2004) Tryptophan substitutions reveal the role of nicotinic acetylcholine receptor alpha-TM3 domain in channel gating: differences between *Torpedo* and muscle-type AChR, *Biochemistry 43*, 78−84.
31. Miyazawa, A., Fujiyoshi, Y., and Unwin, N. (2003) Structure and gating mechanism of the acetylcholine receptor pore, *Nature 424*, 949−955.
32. Görne-Tschelnokw, U., Strecker, A., Kaduk, C., Naumann, D., and Hucho, F. (1994) The transmembrane domains of the nicotinic acetylcholine receptor contain alpha-helical and beta structures, *EMBO J. 13*, 338−341.
33. Méthot, N., Ritchie, B. D., Blanton, M. P., and Baenziger, J. E. (2001) Structure of the pore-forming transmembrane domain of a ligand-gated ion channel, *J. Biol. Chem. 276*, 23726−23732.
34. Lugovskoy, A. A., Maslennikov, I. V., Utkin, Y. N., Tsetlin, V. I., Cohen, J. B., and Arseniev, A. S. (1998) Spatial structure of the M3 transmembrane segment of the nicotinic acetylcholine receptor alpha subunit, *Eur. J. Biochem. 255*, 455−461.
35. Guzman, G. R., Santiago, J., Ricardo, A., Marti-Arbona, R., Rojas, L V., and Lasalde-Dominicci, J. A. (2003) Tryptophan scanning mutagenesis in the alphaM3 transmembrane domain of the *Torpedo californica* acetylcholine receptor: functional and structural implications, *Biochemistry 42*, 12243−12250.
36. Ho, S. N., Hunt, H. D., Horton, R. M., Pullen, J. K., and Pease, L. R. (1989) Site-directed mutagenesis by overlap extension using the polymerase chain reaction, *Gene 77*, 51−59.
37. Pradier, L., Yee, A. S., and McNamee, M. G. (1989) Use of chemical modifications and site-directed mutagenesis to probe the functional role of thiol groups on the gamma subunit of *Torpedo californica* acetylcholine receptor, *Biochemistry 28*, 6562−6571.
38. Gomez, C. M., Maselli, R. A., Groshong, J., Zayas, R., Wollman, R. L., Cens, T., and Charnet, P. (2002) Active calcium accumulation underlies severe weakness in a panel of mice with slow-channel syndrome. *J. Neurosci. 22*, 6447−6457.
39. Tomaselli, G. F., McLaughlin, J. T., Jurman, M. E., Hawrot, E.; Yellen, G. (1991) Mutations affecting agonist sensitivity of the nicotinic acetylcholine receptor, *Biophys. J. 60*, 721−727.
40. McNerNey, M. L., Pardi, D., Pugh, P. C., Nai, Q., and Margiotta, J. F. (2000) Expression and channel properties of alpha-bungarotoxin-sensitive acetylcholine receptors on chick ciliary and choroid neurons, *J. Neurophysiol. 84*, 1314−1329.
41. Treutlein, H. R., Lemmon, M. A., Engelman, D., Brunger, A. T. (1992) The glycophorin A transmembrane domain dimer: Sequence-specific propensity for a right-handed supercoil of helixes, *Biochemistry 31*, 12726−12733.

BI0362368